Estimation of High Velocities in Synthetic-Aperture Imaging—Part II: Experimental Investigation

Jørgen Arendt Jensen, *Fellow, IEEE*

***Abstract*— This paper describes the performance of a new pulse sequence design and estimation approach for increasing the maximum detectable velocity in synthetic aperture (SA) velocity imaging. Measurements are conducted for conventional imaging for comparing the velocity range detectable by a directional transverse oscillation (DTO) autocorrelation estimator to a new cross-correlation estimator. For conventional focused emissions, a 192-element, 3-MHz convex array transducer is used together with the SARUS experimental scanner on a flow rig at beam-to-flow angles of 60°, 70°, and 90°. Here, the new estimator always yields a higher precision, and the aliasing limit is increased by a factor of 3. The new SA interspaced scheme was investigated using Field II simulations and SARUS measurements. A 3-MHz, 128-element phased array was employed with five virtual source emissions scheme for flow estimation and 15 emissions for B-mode imaging. The scheme was interleaved three times for a positive, negative, and positive transmission, so that nonlinear pulse inversion could also be made. The experiments were conducted at three angles and for four different pulse repetition frequencies. A peak transverse velocity of 0.51 m/s could be estimated at $f_{\mathrm{prf}} = 450$ Hz, translating to 5.6 m/s at $f_{\mathrm{prf}} = 5$ kHz showing the theoretical increase of a factor of 10 predicted in the accompanying theory paper.**

***Index Terms*— Synthetic aperture, ultrasound imaging velocity estimation.**

I. Introduction

ESTIMATION of high velocities is of interest in many applications where diseases in the cardiovascular system are found. Velocities are increased proportionally to stenosis degree in vessels, which can result in peak velocities in excess of 2.3 m/s for stenosis of more than 70% in the carotid artery [1]. Such vessels are superficial, and the pulse repetition frequency f_{prf} can often be maintained high above, e.g., 10 kHz. In cardiology, incompetent valves can result in regurgitant jets with velocities up to 7 m/s, which currently have to be diagnosed using continuous wave Doppler systems. This limits the available isolation angles and makes it difficult to select the measurement depth. A full view of the heart with a flexible placement of the interrogation volume would be highly beneficial. This demands $f_{\mathrm{prf}} = 5$ kHz for imaging down to 15 cm, in which current synthetic-aperture (SA) vector flow imaging (VFI) systems usually limit the maximum velocity to around 0.25 m/s for a 3-MHz probe. The aim of this paper is, therefore, to experimentally investigate methods with the capability of measuring velocities up to 3–7 m/s using pulse repetition frequencies of 5–10 kHz for SA VFI.

Methods for increasing the maximum detectable velocity were described in the accompanying paper [2]. The first method relies on a new pulsing scheme for SA VFI. In previous methods, a series of emissions was produced to generate low-resolution images (LRIs), and a high-resolution image (HRI) was then assembled from the LRIs. Repeating the process generates a second HRI to be correlated with the first for estimating the spatial velocity distribution [3]. The correlation between measurements N emissions apart results in an effective pulse repetition frequency of $f_{\mathrm{eff,prf}} = f_{\mathrm{prf}}/N$, which lowers the maximum detectable velocity by a factor of N. Interleaving the sequences for the two or more HRIs reduces the time distance to $1/f_{\mathrm{prf}}$, resulting in the largest maximum detectable velocity possible.

The second method employs a new directional transverse oscillation (DTO) cross-correlation vector flow estimator, which avoids the phase aliasing from the previous autocorrelation method [4], [5]. This can increase the maximum detectable velocity beyond the $\lambda_x f_{\mathrm{prf}}/4$ aliasing limit, where λ_x is the lateral oscillation wavelength. The estimator uses data beamformed orthogonal to the ultrasound propagation direction and cross correlates data along this direction. This makes the estimator independent of the actual value of λ_x, and no calibration has to be performed to yield close to unbiased results.

The new estimator is investigated using flow rig measurements in Section IV, where the autocorrelation and cross-correlation estimates are compared using conventional duplex ultrasound data. The new estimator is combined with the interleaved SA sequence in Section V for a phased array probe, and the performance found for both simulated and measured data.

II. Measurement Setup for Conventional Imaging

A convex array transducer with 192 elements and a center frequency of 3 MHz is used for the measurements in conjunction with the SARUS ultrasound scanner [6]. A duplex sequence is used, as described in [5]. A circulating flow rig with a 6-mm-radius tube was scanned, and the volume flow recorded by a Danfoss Magnetic flowmeter MAG1100 (Danfoss, Nordborg, Denmark). The volume flow was 106.4 l/h corresponding to a peak velocity in the vessel of 0.52 m/s assuming a fully developed parabolic profile. The beam-to-flow angles were 60°, 75°, and 90°, and the measurement

Manuscript received July 22, 2018; accepted March 15, 2019. Date of publication March 20, 2019; date of current version June 5, 2019.

The author is with the Center for Fast Ultrasound Imaging, Department of Electrical Engineering, Technical University of Denmark, 2800 Kongens Lyngby, Denmark (e-mail: jaj@elektro.dtu.dk).

Digital Object Identifier 10.1109/TUFFC.2019.2906390

0885-3010 © 2019 IEEE. Personal use is permitted, but republication/redistribution requires IEEE permission.
See http://www.ieee.org/publications_standards/publications/rights/index.html for more information.

TABLE I
PARAMETERS USED FOR THE DUPLEX TO MEASUREMENTS

Parameter	Value	Unit	Variable
Transducer elements	192		
Center frequency	3.0	MHz	f_0
Cycles in transmit pulse	4		
Transmit apodization	von Hann		
Element pitch	0.33	mm	P_i
Element height	13	mm	
Elevation focus	65	mm	
Convex radius	60	mm	
Transmit focus for vessel depths below 80 mm	105	mm	
Transmit focus for vessel depths beyond 80 mm	300	mm	
Pulse repetition frequency	2.5	kHz	f_{prf}
Active transmit elements	64		
Measurement sampling frequency	17.5	MHz	

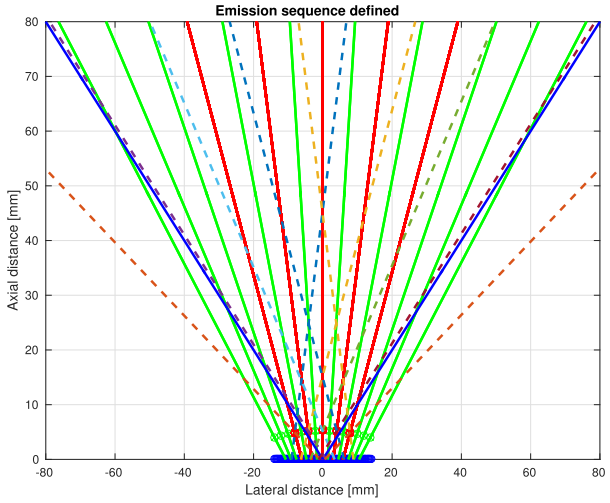

Fig. 1. Geometric depiction of the SA flow imaging sequence. Red circles: virtual source position for flow emissions. Green circles: B-mode emissions. Solid lines: directions for the emissions. Dashed lines: acceptance angle used in the beamformation. Blue solid lines: possible imaging region.

depths varied from 24 to 156 mm. The data are identical to the ones used in [5], and all parameters are shown in Table I.

III. MEASUREMENT SETUP FOR INTERLEAVED SA DTO

A phased array transducer with 128 elements and a center frequency of 3 MHz is used for the measurements in conjunction with the SARUS ultrasound scanner [6]. The emission sequence contains both B-mode and flow emissions as shown in Fig. 1, and the polarity of the emissions is also inverted, so that pulse inversion imaging can be made. The pulse inversion is emitted in a short sequence and the B-mode emissions are interspaced between the blocks of flow emissions as shown in Table II. The positions of different emitted virtual sources and their directions are shown in Fig. 1.

In Table II, $-v_2^{(1)}$ denotes a negative excitation waveform emission in direction 2 for the first time, and $+B_{15}^{(1)}$ denotes a positive B-mode emission in direction 15. Fifteen emissions are emitted for a full B-mode image, and five emissions are used for creating an HRI for velocity estimation. Five of the velocity emissions are also used in forming the B-mode image, and there are, thus, ten blocks of emissions starting with two B-mode emissions (positive and negative for the same virtual source) followed by three times five-flow emissions.

The scheme makes it possible to perform pulse inversion imaging. It also makes it possible to correlate HRIs created from $+v_{1\cdots5}^{(1)}$ with $+v_{1\cdots5}^{(3)}$, which has only a time difference of 2 T_{prf}. Alternatively, sequences like $+v_{1\cdots5}^{(1)} - v_{1\cdots5}^{(2)}$ could be correlated with $+v_{1\cdots5}^{(3)} - v_{1\cdots5}^{(2)}$. Another possibility is to change the sign of the negative emission $-v_1^{(2)}$ to make the time difference equal to T_{prf}, which increases the maximum detectable velocity by a factor of 2.

The same circulating flow rig setup as described in Section II was used for the measurements. All parameters are shown in Table III. Simulations using Field II [7], [8] were conducted with the exact same transducer parameters, interspacing, and acquisition parameters. The impulse response of the probe was used, but no nonlinear effects were introduced in the entirely linear simulation.

A. Stationary Echo Canceling Filters

Stationary echo canceling was performed by subtracting the mean signal. The mean signal was calculated across all HRIs used for velocity estimation, and it was subsequently subtracted from the individual HRIs. The same echo canceling approach was also employed for the measurements described in Section II. Other more advanced schemes based on decomposition could be used [9]–[14]. This is, however, not necessary here, as all data employed are either simulated or measured in a flow rig, whether tissue motion is not present.

IV. RESULTS FOR DTO ESTIMATORS

The autocorrelation DTO estimator described in [5] was used as a reference. It uses beamformed data measured using SARUS with TO receive apodization and focusing in a line perpendicular to the ultrasound propagation direction. This data are used in the estimator to yield the lateral velocity component. The same beamformed data are used in the new cross-correlation estimator developed in the accompanying paper [2].

A. Estimation for Different Angles

The performance of the cross-correlation approach compared to autocorrelation DTO can be seen in Fig. 2, where 32 emissions have been used for imaging the vessel at a depth of 64 mm and a beam-to-flow angle of 90°. The true profile is shown as the green dashed line, and the mean of all estimated profiles is shown as the blue curve ± 1 standard deviation (SD). Velocity estimates outside the vessel boundary vary widely, as no discriminator has been applied. The overall statistics has, therefore, been calculated on the central 90% of the vessel to avoid the influence from the echo canceling filter [10], [15] at the boundary and outside

TABLE II

EMISSION SEQUENCE FOR THE SA B-MODE/FLOW SEQUENCE AND THE CORRESPONDING LRI AND HRI. THE LEFT SIDE SHOWS THE EMISSION SEQUENCE AND THE RIGHT SIDE SHOWS THE CORRESPONDING LRIS AND THEIR SUMMATION TO HRIS

Emission 1	Emission 2	Emission 3	Low resolution images:		
$+B_1^{(1)}$	$-B_1^{(2)}$		$+\text{LRI}_{B_1}^{(1)}$	$-\text{LRI}_{B_1}^{(2)}$	
$+v_1^{(1)}$	$-v_1^{(2)}$	$+v_1^{(3)}$	$+\text{LRI}_1^{(1)}$	$-\text{LRI}_1^{(2)}$	$+\text{LRI}_1^{(3)}$
$+v_2^{(1)}$	$-v_2^{(2)}$	$+v_2^{(3)}$	$+\text{LRI}_2^{(1)}$	$-\text{LRI}_2^{(2)}$	$+\text{LRI}_2^{(3)}$
$+v_3^{(1)}$	$-v_3^{(2)}$	$+v_3^{(3)}$	$+\text{LRI}_3^{(1)}$	$-\text{LRI}_3^{(2)}$	$+\text{LRI}_3^{(3)}$
$+v_4^{(1)}$	$-v_4^{(2)}$	$+v_4^{(3)}$	$+\text{LRI}_4^{(1)}$	$-\text{LRI}_4^{(2)}$	$+\text{LRI}_4^{(3)}$
$+v_5^{(1)}$	$-v_5^{(2)}$	$+v_5^{(3)}$	$+\text{LRI}_5^{(1)}$	$-\text{LRI}_5^{(2)}$	$+\text{LRI}_5^{(3)}$
		LRIs sums to:	$\sum_{i=1}^{5}+\text{LRI}_i^{(1)}$ = $+\text{HRI}^{(1v)}$	$\sum_{i=1}^{5}-\text{LRI}_i^{(2)}$ = $-\text{HRI}^{(2v)}$	$\sum_{i=1}^{5}+\text{LRI}_i^{(3)}$ = $+\text{HRI}^{(3v)}$
$+B_2^{(1)}$	$-B_2^{(2)}$		$+\text{LRI}_{B_2}^{(1)}$	$-\text{LRI}_{B_2}^{(2)}$	
$+v_1^{(4)}$	$-v_1^{(5)}$	$+v_1^{(6)}$	$+\text{LRI}_1^{(4)}$	$-\text{LRI}_1^{(5)}$	$+\text{LRI}_1^{(6)}$
$+v_2^{(4)}$	$-v_2^{(5)}$	$+v_2^{(6)}$	$+\text{LRI}_2^{(4)}$	$-\text{LRI}_2^{(5)}$	$+\text{LRI}_2^{(6)}$
$+v_3^{(4)}$	$-v_3^{(5)}$	$+v_3^{(6)}$	$+\text{LRI}_3^{(4)}$	$-\text{LRI}_3^{(5)}$	$+\text{LRI}_3^{(6)}$
$+v_4^{(4)}$	$-v_4^{(5)}$	$+v_4^{(6)}$	$+\text{LRI}_4^{(4)}$	$-\text{LRI}_4^{(5)}$	$+\text{LRI}_4^{(6)}$
$+v_5^{(4)}$	$-v_5^{(5)}$	$+v_5^{(6)}$	$+\text{LRI}_5^{(4)}$	$-\text{LRI}_5^{(5)}$	$+\text{LRI}_5^{(6)}$
		LRIs sums to:	$\sum_{i=1}^{5}+\text{LRI}_i^{(4)}$ = $+\text{HRI}^{(4v)}$	$\sum_{i=1}^{5}-\text{LRI}_i^{(5)}$ = $-\text{HRI}^{(5v)}$	$\sum_{i=1}^{5}+\text{LRI}_i^{(6)}$ = $+\text{HRI}^{(6v)}$
$\vdots$	$\vdots$	$\vdots$			
$+B_{15}^{(1)}$	$-B_{15}^{(2)}$		$+\text{LRI}_{B_{15}}^{(1)}$	$-\text{LRI}_{B_{15}}^{(2)}$	
$+v_1^{(28)}$	$-v_1^{(29)}$	$-v_1^{(30)}$	$+\text{LRI}_1^{(28)}$	$-\text{LRI}_1^{(29)}$	$+\text{LRI}_1^{(30)}$
$\vdots$	$\vdots$	$\vdots$			
			B-mode emissions sums to:		
			$\sum_{i=1}^{10}+\text{LRI}_{B_j}^{(1)}+\sum_{i=1}^{5}+\text{LRI}_i^{(1)}$ = $+\text{HRI}^{(1B)}$	$\sum_{i=1}^{10}-\text{LRI}_{B_j}^{(2)}+\sum_{i=1}^{5}-\text{LRI}_i^{(2)}$ = $-\text{HRI}^{(2B)}$	

TABLE III

PARAMETERS USED FOR THE SA INTERLEAVED MEASUREMENTS

Parameter	**Value**	**Unit**	**Variable**
Transducer elements	128		
Center frequency	4.0	MHz	f_0
Transmit frequency	2.7	MHz	
Cycles in transmit pulse	2		
Transmit apodization	von Hann		
Element pitch	0.22	mm	P_i
Element height	15	mm	
Elevation focus	85	mm	
Active transmit elements	32		
Focal depth	5.74	mm	
Measurement sampling frequency	17.5	MHz	
Simulation sampling frequency	350	MHz	
Flow angles	60, 70, 90	°	
Pulse repetition frequencies	225, 450		
	1000, 4500	Hz	f_{prf}

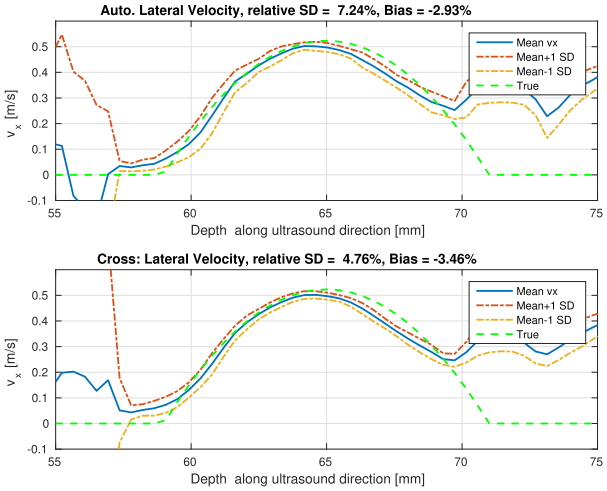

Fig. 2. Estimated mean velocity profiles for the DTO autocorrelation approach (top) and for the cross-correlation method (bottom) at a beam-to-flow angle of 90° using 32 emissions.

the vessel. For DTO, the relative SD is 7.24%, whereas it is 4.76% for the cross-correlation approach. The bias levels are similar, showing that the new estimator has a slight advantage compared to DTO in performance.

Estimates for a beam-to-flow angle of 60° are shown in Fig. 3. There is, thus, a significant axial component, which is compensated out in the estimator. Again, the SD is slightly lower for the new method compared to DTO as shown on the

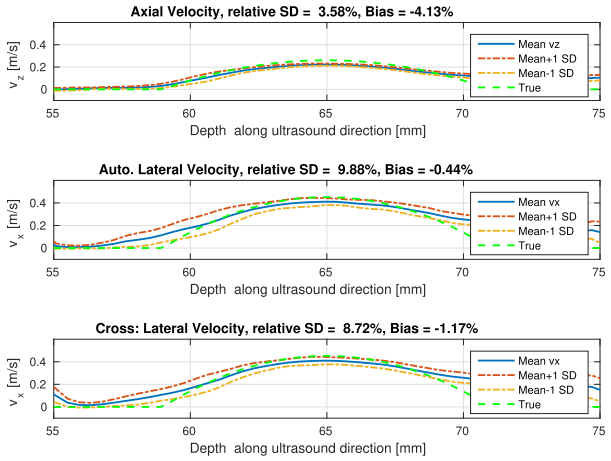

Fig. 3. Estimated mean velocity profiles for the DTO approach for the axial velocity (top), the lateral velocity using the autocorrelation approach (middle), and the cross-correlation method (bottom) at a beam-to-flow angle of 60°.

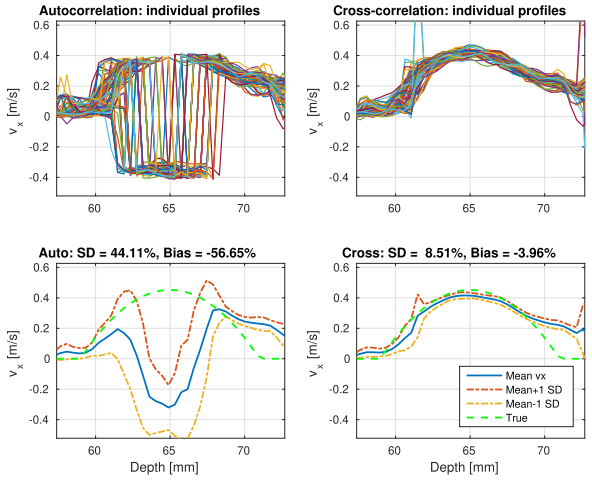

Fig. 4. Velocity profiles as shown on the top graphs for the autocorrelation (left) and the cross-correlation (right) DTO estimators, when f_{prf} is reduced by a factor of 4 to 650 Hz. The mean velocity profiles ± SD are shown in the bottom graphs.

top plots. It should be noted that the same autocorrelation estimator is used for both methods for the axial velocity component.

B. Increased Velocity Range

Fig. 4 demonstrates the larger velocity range for the cross-correlation method. The pulse repetition frequency f_{prf} was lowered by a factor of 4 by using every fourth line in the estimation process. Estimates at the vessel center are aliased for the autocorrelation estimator in the top graph, whereas the cross-correlation estimator still can find reliable estimates. The vessel was placed at 65 mm, the beam-to-flow angle was 60°, and 32 emissions were used in the estimator.

The lateral wavelength λ_x used was 2.39 mm, and f_{prf} was 2.5 kHz giving an aliasing limit of $v_{z,\max} = \lambda_x f_{\text{prf}}/4 = 1.49$ m/s. Reducing f_{prf} by a factor N, thus reduces $v_{z,\max}$ by this factor to 0.373 m/s. Fig. 4 shows that this limit applies for the autocorrelation estimator, but the new DTO cross-correlation estimator can still provide the correct velocity estimate.

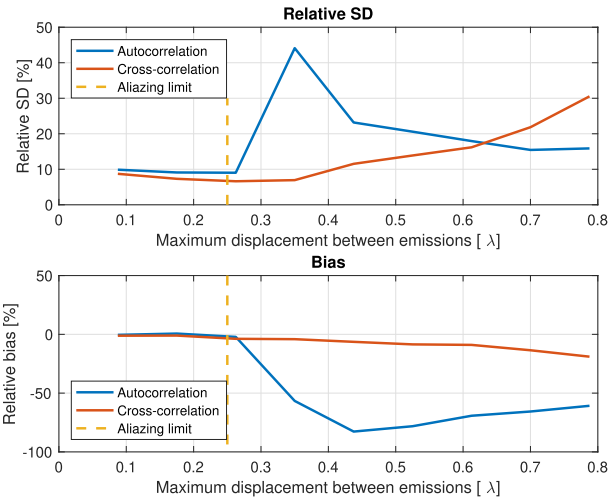

Fig. 5. SD (top) and bias (bottom) as a function of displacement between pulse emissions in wavelengths for the autocorrelation (blue) and the cross-correlation (red) estimators, when the effective f_{prf} is varied.

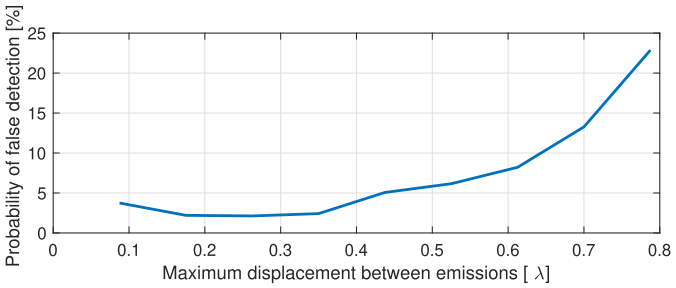

Fig. 6. Probability of false detection for the cross-correlation estimator.

The bias and SD are heavily influenced by aliasing, and the limit for the new estimator can therefore be determined using the bias increase as shown in Fig. 5. Here, the number of skipped lines N is varied, resulting in a larger displacement between correlated lines. This is expressed in wavelengths of motions between emissions. The autocorrelation DTO estimator has an aliasing limit of $\lambda_x/4$ as indicated by the dashed yellow line. Bias and SD increase for the autocorrelation estimates after this aliasing limit, whereas the bias is relatively constant for the cross-correlation estimator up to $0.75\lambda_x$, three times higher than for the autocorrelation estimator. The SD rises slightly for increasing displacement values due to the increased probability of false detection at higher search ranges [16]. This is shown in Fig. 6, calculated as estimates which deviates more than one-tenth of the peak velocity from the correct velocity. Probabilities below 20% are sparse enough that they can be compensated for either visually or through considering adjacent estimates to correct outliers [17]. This gives a limit around $0.75\lambda_x$ corresponding to 9 m/s, if $f_{\text{prf}} = 5$ kHz. The SD is also affected by the false peaks, and this is the main reason for the increase in SD for velocities higher than 5 m/s corresponding to motions beyond $0.4\lambda_x$ per emission.

C. Performance Comparison

Fig. 7 shows the performance as a function of emissions used for the estimates at a beam-to-flow angle of 60° and

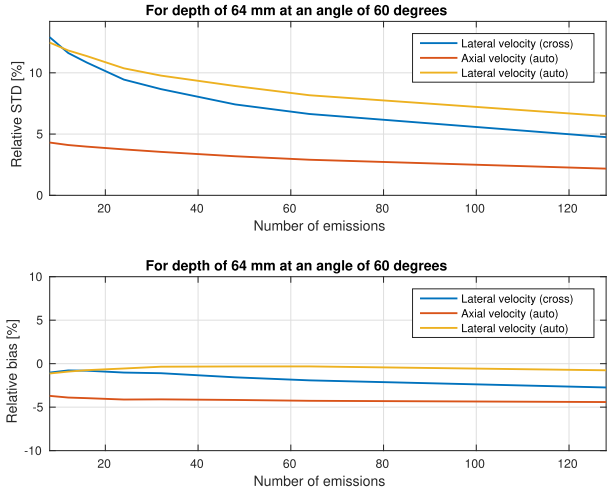

Fig. 7. Performance as a function of emissions used for the estimates at a beam-to-flow angle of 60° and a vessel depth of 64 mm.

a vessel depth of 64 mm. The relative SD is shown on the top and the bias on the bottom graph. The red color indicates estimates from the new cross-correlation approach, and the orange color is for DTO. The relative SD is in all cases lower for the cross-correlation approach demonstrating that a better precision is attained for the same number of emissions using exactly the same beamformed data.

V. Results for Interleaved SA DTO

The sequence described in Section III has been used to acquire data from the flow rig for different values of f_{prf} and for different beam-to-flow angles. Eight HRIs were used for the interleaved sequence. Echo canceling was performed by subtracting the mean value of the HRIs from the data. Three HRIs were created in one sequence by combining all the first positive emission in $+\text{HRI}^{(1v)}$, then all negative emissions in $-\text{HRI}^{(2v)}$, and finally all of the last positive emissions in $+\text{HRI}^{(3v)}$. Correlation was then conducted between $+\text{HRI}^{(1v)}$ and $+\text{HRI}^{(2v)}$ and between $+\text{HRI}^{(2v)}$ and $+\text{HRI}^{(3v)}$. The correlation functions were averaged across all the HRIs. The scheme maintains the shortest time difference between correlated signals, yields data that can be beamformed everywhere in the images, and is continuous in time. The data shown here span $8 \times (3{\times}5{+}2) = 136$ emissions, which are comparable to the normal time span of a spectral velocity estimate, which often uses 128 emissions.

The first measurement uses $f_{\text{prf}} = 4500$ Hz and the second uses only a 450-Hz f_{prf}. The peak velocity in the vessel is 0.52 m/s. Fig. 8 shows the estimated velocity profiles. The SD of the lateral velocity component is maintained around 2.5% in both cases although the time between correlations is increased by a factor of 10. For a normal SA flow sequence, the distance between HRIs to correlate would, here, be 17 emissions, where it now is only one emission. The largest velocity possible to estimate in the lower sequence would then be above 0.52 m/s and scaling f_{prf} to 4500 Hz gives a maximum velocity of 5.2 m/s. Using even higher pulse repetition frequencies can further increase the maximum detectable velocity. It should also be noted that the data are continuously available in the full imaging region shown in Fig. 1. It is, therefore, also possible

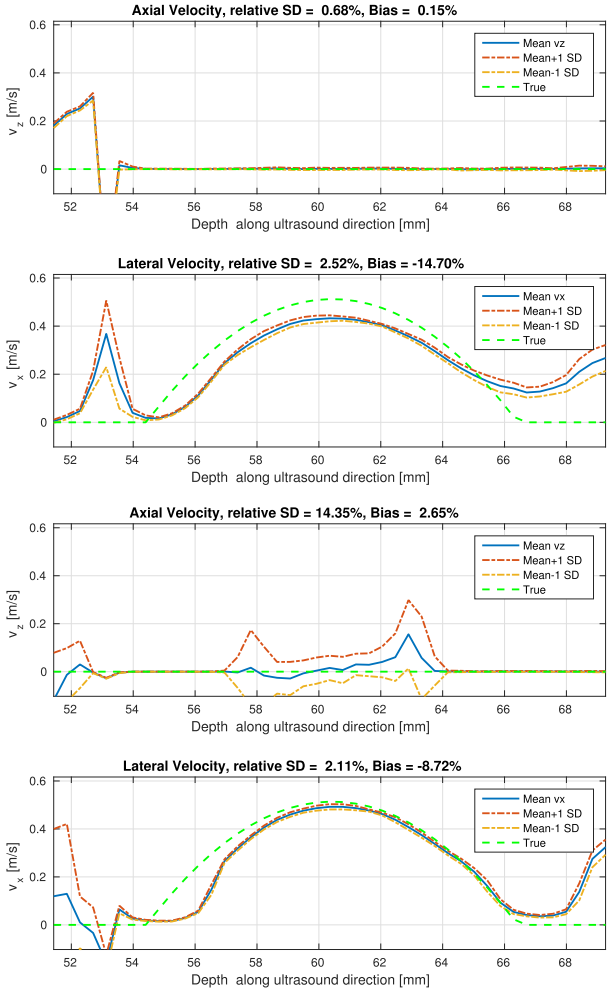

Fig. 8. Mean velocity profiles ± SD for SA VFI using a 4500-Hz f_{prf} (top) and a 450-Hz f_{prf} (bottom) at a beam-to-flow angle of 90°.

to estimate low velocities as averaging can take place over as long time as the velocity can be considered stationary. This also makes echo canceling much easier, as any echo canceling filter can be employed for the continuous data.

The velocity estimation has been conducted for different pulse repetition frequencies of 225, 450, 1000, and 4500 Hz and for beam-to-flow angles of 60°, 75°, and 90°. Directional data orthogonal to the imaging direction has been beamformed using TO, and data have also been beamformed along the flow directional to enable the use of directional cross-correlation estimation of the velocity. The results for the DTO estimates are shown in Fig. 9 for the measured data. A fairly low bias and SD is maintained for both $f_{\text{prf}} = 4500$ Hz and $f_{\text{prf}} = 1000$ Hz, whereas the results deteriorate significantly for $f_{\text{prf}} = 450$ Hz at angles of 60° and 75°. Scaling f_{prf} to 5 kHz for the 1-kHz case corresponds to a peak velocity in the vessel of 2.6 m/s.

The same pattern is seen for the simulated data in Fig. 10, although with a slightly lower bias and SD. The maximum detectable velocity can be increased by using directional data focused along the flow direction [18], [19], where the results from simulations are shown in Fig. 11. The SD is now significantly lower around 1% and reliable velocities can be

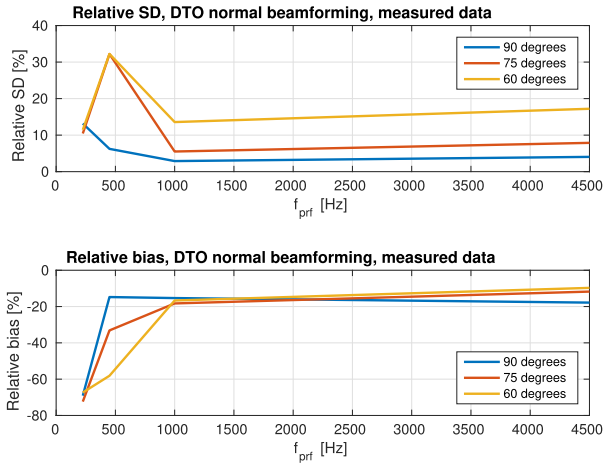

Fig. 9. Performance for SA imaging using the DTO cross-correlation estimator as a function of f_{prf} for the measured data.

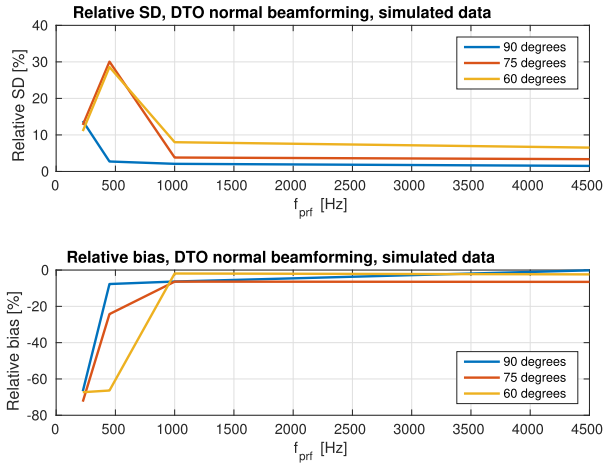

Fig. 10. Performance for SA imaging using the DTO cross-correlation estimator as a function of f_{prf} for the simulated data.

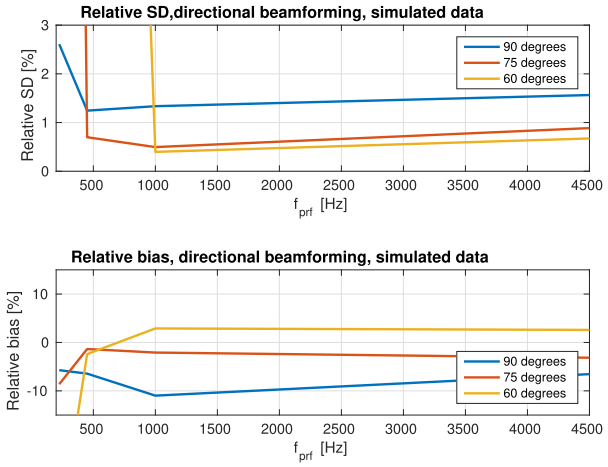

Fig. 11. Performance for SA imaging using the directional cross-correlation estimator as a function of f_{prf} for the simulated data.

estimated at both 75° and 90°. Scaling f_{prf} from 450 Hz to 5 kHz in this case corresponds to a peak velocity in the vessel of 5.8 m/s. At 90° the profile can still be estimated with a relative SD of 2.6% and bias of 5.7% for $f_{\text{prf}} = 225$ Hz. For 10 kHz f_{prf}, this translates to peak velocities of 23.1 m/s. For the other angles, there is a significant amount of false detections, which could be potentially corrected to yield the true value by employing clustering [17] or regularization [20].

VI. Conclusion

A new approach for vector flow estimation using transverse oscillation (TO) and lateral beamforming in combination with cross correlation was developed and investigated. A new preprocessing step removes the influence from the axial velocity component and makes it possible to decompose the estimation into an axial and a lateral cross-correlation estimator. The advantages are a significantly higher maximum detectable velocity and a slightly improved SD on the results improving on the estimates for the same number of data. The estimate is also self-calibrating, as no estimation of the lateral oscillation wavelength λ_x is needed, resulting in a low bias. Flow rig measurements using a duplex setup for a convex probe demonstrated that the relative SD is between 4.8% and 8.7% and the bias is between −3.5% and −1.2% at angles from 60° to 90° when using 32 emissions at $f_{\text{prf}} = 2.5$ kHz. The new estimator goes beyond the normal aliasing limit of $\lambda_x f_{\text{prf}}/4$ and could, therefore, estimate considerably higher velocities. Peak velocities up to 9 m/s could be estimated at $f_{\text{prf}} = 5$ kHz with a probability of false detection around 20%, which is visually acceptable or could be corrected by clustering estimates over time or space to correct false values. The peak detection is, thus, three times higher than for the autocorrelation estimator.

An interleaved pulse emission scheme for SA flow imaging makes it possible to maintain the highest possible maximum detectable velocity in an SA sequence with multiple emissions. This decouples the link between the sequence length N and the maximum detectable velocity. Long sequences with good focusing properties and low side lobes can be used and at the same time maintain the highest possible maximum detectable velocity. Continuous data are obtained, which yield a low SD, arbitrary echo canceling possibilities, and the ability to detect low velocities. The sequence investigated contained a flow sequence interleaved with a longer B-mode sequence. The flow sequence used five virtual sources, where each source was repeated with a positive, negative, and positive polarity emission. This makes it possible to perform velocity estimation and B-mode imaging with pulse inversion for both. Two different velocity estimation schemes were implemented using DTO and directional beamforming along the flow direction, and they were evaluated using a combination of eight HRIs. Satisfactory performance was obtained for both methods using f_{prf} of 4.5 and 1 kHz. The bias and SD were lower for the simulated data indicating a bit more noise in the measured data. The performance was significantly better for the directionally focused data and SD below 1.5% was obtained with a bias below 5% down to f_{prf} of 450 Hz. Acceptable results could even be obtained at $f_{\text{prf}} = 225$ Hz at a beam-to-flow angle of 90°. This, however, assumes a known beam-to-flow angle, if significantly more beamforming is to be avoided in the directional approach to estimate the angle. A combination of DTO autocorrelation and directional estimation has been made for plane wave imaging, and this reduces the beamforming demands significantly [21].

These results indicate a peak detectable velocity of at least 2.9 m/s for the DTO method and 5.8 m/s for the directional approach, when $f_{\text{prf}} = 5$ kHz is used. This is lower than for the duplex sequence, and this is due to the combination of five emissions in SA before the velocity is estimated. Compensation for the motion could also be introduced [22], and this might, in certain cases, improve on the estimates. The profiles detected for lower values of f_{prf} have high SDs due to many false peak detections. These can be removed using clustering [17] or regularization [20]. The peak velocity can also be increased by using $f_{\text{prf}} = 10$ kHz, resulting in a maximum detectable velocity of 23.1 m/s for directional beamforming and cross correlation at 90°. Another approach is to increase the lateral wavelength, which will also proportionally increase the maximum detectable velocity. The axial velocity is more difficult to estimate for high velocities as the wavelength is small and cannot be easily manipulated. For high velocities, the transducer should, therefore, be oriented, so that the main velocity component is along the transverse direction to reduce the axial velocity component.

The demand enforced in cardiology for visualizing the whole heart is $f_{\text{prf}} = 5$ kHz to scan down to depths of 15 cm. Regurgitation jets can yield velocities up to 7 m/s and today have to be measured by continuous wave Doppler. This creates ambiguity with regard to depth and angle and, thus, actual value of the velocity. The methods presented here open the possibility of scanning the heart from new angles and yield the true peak velocity and the direction of the flow without ambiguity at more than 60 independent frames per second.

REFERENCES

[1] E. G. Grant *et al.*, "Carotid artery stenosis: Gray-scale and Doppler us diagnosis—Society of radiologists in ultrasound consensus conference," *Radiology*, vol. 229, no. 2, pp. 340–346, 2003.

[2] J. A. Jensen, "Estimation of high velocities in synthetic aperture imaging: I: Theory," *IEEE Trans. Ultrason., Ferroelectr., Freq. Control*, vol. 66, no. 6, pp. 1024–2031, Jun. 2019.

[3] S. I. Nikolov and J. A. Jensen, "*In-vivo* synthetic aperture flow imaging in medical ultrasound," *IEEE Trans. Ultrason., Ferroelectr., Freq. Control*, vol. 50, no. 7, pp. 848–856, Jul. 2003.

[4] J. A. Jensen, "A new estimator for vector velocity estimation," *IEEE Trans. Ultrason., Ferroelectr., Freq. Control*, vol. 48, no. 4, pp. 886–894, Jul. 2001.

[5] J. A. Jensen, "Directional transverse oscillation vector flow estimation," *IEEE Trans. Ultrason., Ferroelectr., Freq. Control*, vol. 64, no. 8, pp. 1194–1204, Aug. 2017.

[6] J. A. Jensen *et al.*, "SARUS: A synthetic aperture real-time ultrasound system," *IEEE Trans. Ultrason., Ferroelectr., Freq. Control*, vol. 60, no. 9, pp. 1838–1852, Sep. 2013.

[7] J. A. Jensen and N. B. Svendsen, "Calculation of pressure fields from arbitrarily shaped, apodized, and excited ultrasound transducers," *IEEE Trans. Ultrason., Ferroelectr., Freq. Control*, vol. 39, no. 2, pp. 262–267, Mar. 1992.

[8] J. A. Jensen, "Field: A program for simulating ultrasound systems," in *Proc. 10th Nordicbaltic Conf. Biomed. Imag.*, vol. 4, 1996, pp. 351–353.

[9] L. A. F. Ledoux, P. J. Brands, and A. P. G. Hoeks, "Reduction of the clutter component in Doppler ultrasound signals based on singular value decomposition: A simulation study," *Ultrason. Imag.*, 1997, pp. 1–18.

[10] S. Bjaerum, H. Torp, and K. Kristoffersen, "Clutter filter design for ultrasound color flow imaging," *IEEE Trans. Ultrason., Ferroelectr., Freq. Control*, vol. 49, no. 2, pp. 204–216, Feb. 2002.

[11] L. Lovstakken, S. Bjaerum, K. Kristoffersen, R. Haaverstad, and H. Torp, "Real-time adaptive clutter rejection filtering in color flow imaging using power method iterations," *IEEE Trans. Ultrason., Ferroelectr., Freq. Control*, vol. 53, no. 9, pp. 1597–1608, Sep. 2006.

[12] A. C. H. Yu and L. Lovstakken, "Eigen-based clutter filter design for ultrasound color flow imaging: A review," *IEEE Trans. Ultrason., Ferroelectr., Freq. Control*, vol. 57, no. 5, pp. 1096–1111, May 2010.

[13] C. Demené *et al.*, "Spatiotemporal clutter filtering of ultrafast ultrasound data highly increases Doppler and fultrasound sensitivity," *IEEE Trans. Med. Imag.*, vol. 34, no. 11, pp. 2271–2285, Nov. 2015.

[14] J. Baranger, B. Arnal, F. Perren, O. Baud, M. Tanter, and C. Demené, "Adaptive spatiotemporal SVD clutter filtering for ultrafast Doppler imaging using similarity of spatial singular vectors," *IEEE Trans. Med. Imag.*, vol. 37, no. 7, pp. 1574–1586, Jul. 2018.

[15] D. H. Evans and W. N. McDicken, *Doppler Ultrasound: Physics, Instrumentation and Signal Processing*. New York, NY, USA: Wiley, 2000.

[16] J. A. Jensen, *Estimation of Blood Velocities Using Ultrasound: A Signal Processing Approach*. New York, NY, USA: Cambridge Univ., 1996.

[17] J. A. Jensen, "Range/velocity limitations for time-domain blood velocity estimation," *Ultrasound Med. Biol.*, vol. 19, no. 9, pp. 741–749, 1993.

[18] J. A. Jensen, "Directional velocity estimation using focusing along the flow direction. I: Theory and simulation," *IEEE Trans. Ultrason., Ferroelectr., Freq. Control*, vol. 50, no. 7, pp. 857–872, Jul. 2003.

[19] J. A. Jensen and R. Bjerngaard, "Directional velocity estimation using focusing along the flow direction. II: Experimental investigation," *IEEE Trans. Ultrason., Ferroelectr., Freq. Control*, vol. 50, no. 7, pp. 873–880, Jul. 2003.

[20] D. H. Iversen, F. Lindseth, G. Unsgaard, H. Torp, and L. Lovstakken, "Model-based correction of velocity measurements in navigated 3-D ultrasound imaging during neurosurgical interventions," *IEEE Trans. Med. Imag.*, vol. 32, no. 9, pp. 1622–1631, Sep. 2013.

[21] J. Jensen, C. A. V. Hoyos, M. B. Stuart, C. Ewertsen, M. B. Nielsen, and J. A. Jensen, "Fast plane wave 2-D vector flow imaging using transverse oscillation and directional beamforming," *IEEE Trans. Ultrason., Ferroelectr., Freq. Control*, vol. 64, no. 7, pp. 1050–1062, Jul. 2017.

[22] N. Oddershede and J. A. Jensen, "Effects influencing focusing in synthetic aperture vector flow imaging," *IEEE Trans. Ultrason., Ferroelectr., Freq. Control*, vol. 54, no. 9, pp. 1811–1825, Sep. 2007.

Jørgen Arendt Jensen (M'93–SM'02–F'12) received the M.Sc., Ph.D., and Dr.Techn. degrees from the Technical University of Denmark (DTU), Lyngby, Denmark, in 1985, 1989, and 1996, respectively.

In 2003, he was one of the founders of the Biomedical Engineering Program in medicine and technology, which is a joint degree program between the Technical University of Denmark and the Faculty of Health and Medical Sciences at the University of Copenhagen, Copenhagen, Denmark. The degree is one of the most sought-after engineering degrees in Denmark. He was the Chairman of the study board, from 2003 to 2010. He was an Adjunct Professor with the University of Copenhagen, from 2005 to 2010. He was the Founder and the Head of the Biomedical Engineering Group, DTU, from 2007 to 2010. Since 1993, he has been a Full Professor of biomedical signal processing with the Department of Health Technology, Technical University of Denmark. He has been the Founder and the Head of the Center for Fast Ultrasound Imaging (CFU), Lyngby, since its inauguration in 1998. CFU has contributed with innovations in transverse oscillation vector flow imaging, synthetic aperture flow imaging in 2-D and 3-D, ultrasound simulation, research scanners, and row–column probes and beamforming. He is currently the Developer and Maintainer of the Field II Simulation Program. He has been a Visiting Scientist at Duke University, Durham, NC, USA; Stanford University, Stanford, CA, USA; and the University of Illinois at Urbana–Champaign, IL, USA. He has authored or coauthored more than 450 journal and conference papers on signal processing and medical ultrasound, and the book *Estimation of Blood Velocities Using Ultrasound* (Cambridge University Press, 1996). He has given a number of short courses on simulation, synthetic-aperture imaging, and flow estimation at international scientific conferences and teaches biomedical signal processing and medical imaging at the Technical University of Denmark. His research is centered around the simulation of ultrasound imaging, synthetic-aperture imaging, vector blood flow estimation, 3-D imaging, row–column probes, and construction of ultrasound research systems.

Dr. Jensen has given more than 60 invited talks at international meetings and received several awards for his research, most recently the Grand Solutions Prize from the Danish Minister of Science and the order of the Dannebrog by her Majesty the Queen of Denmark.